

Robust Quantum-Based Interatomic Potentials for Multiscale Modeling in Transition Metals

John A. Moriarty, Lorin X. Benedict, James N. Glosli, Randolph Q. Hood, Daniel A. Orlikowski, Mehul V. Patel, Per Söderlind, Frederick H. Streitz, Meijie Tang and Lin H. Yang

This article has been submitted to the Journal of Materials Research

U.S. Department of Energy

Lawrence
Livermore
National
Laboratory

September 28, 2005

DISCLAIMER

This document was prepared as an account of work sponsored by an agency of the United States Government. Neither the United States Government nor the University of California nor any of their employees, makes any warranty, express or implied, or assumes any legal liability or responsibility for the accuracy, completeness, or usefulness of any information, apparatus, product, or process disclosed, or represents that its use would not infringe privately owned rights. Reference herein to any specific commercial product, process, or service by trade name, trademark, manufacturer, or otherwise, does not necessarily constitute or imply its endorsement, recommendation, or favoring by the United States Government or the University of California. The views and opinions of authors expressed herein do not necessarily state or reflect those of the United States Government or the University of California, and shall not be used for advertising or product endorsement purposes.

This is a preprint of a paper intended for publication in a journal or proceedings. Since changes may be made before publication, this preprint is made available with the understanding that it will not be cited or reproduced without the permission of the author.

Robust Quantum-Based Interatomic Potentials for Multiscale Modeling in Transition Metals

John A. Moriarty, Lorin X. Benedict, James N. Glosli, Randolph Q. Hood, Daniel A. Orlikowski, Mehul V. Patel, Per Söderlind, Frederick H. Streitz, Meijie Tang and Lin H. Yang

Lawrence Livermore National Laboratory, University of California
Livermore, CA 94551-0808, U.S.A.

ABSTRACT

First-principles generalized pseudopotential theory (GPT) provides a fundamental basis for *transferable* multi-ion interatomic potentials in transition metals and alloys within density-functional quantum mechanics. In the central bcc metals, where multi-ion angular forces are important to materials properties, simplified *model* GPT or MGPT potentials have been developed based on canonical *d* bands to allow analytic forms and large-scale atomistic simulations. Robust, advanced-generation MGPT potentials have now been obtained for Ta and Mo and successfully applied to a wide range of structural, thermodynamic, defect and mechanical properties at both ambient and extreme conditions. Selected applications to multiscale modeling discussed here include dislocation core structure and mobility, atomistically informed dislocation dynamics simulations of plasticity, and thermoelasticity and high-pressure strength modeling. Recent algorithm improvements have provided a more general matrix representation of MGPT beyond canonical bands, allowing improved accuracy and extension to *f*-electron actinide metals, an order of magnitude increase in computational speed for dynamic simulations, and the development of temperature-dependent potentials.

I. INTRODUCTION

The prospect of modeling across length scales all the way from the atomic to the continuum level to achieve a predictive multiscale description of mechanical properties such as plasticity and strength has attracted widespread research interest in the last decade [1]. One of the most fundamental and important problems in such multiscale modeling is that of bridging the gap between first-principles quantum mechanics, from which true predictive power for real materials emanates, and the large-scale atomistic simulation of thousands or millions of atoms, which is usually essential to describe the complex atomic processes that link to higher length and time scales. For example, to model single-crystal plasticity at micron length scales via dislocation-dynamics (DD) simulations that evolve the detailed dislocation microstructure requires accurate large-scale atomistic information on the mobility and interaction of individual dislocations. As indicated in Fig. 1, there currently exists a wide spectrum of atomic-scale simulation methods in condensed-matter and materials physics, extending from essentially exact

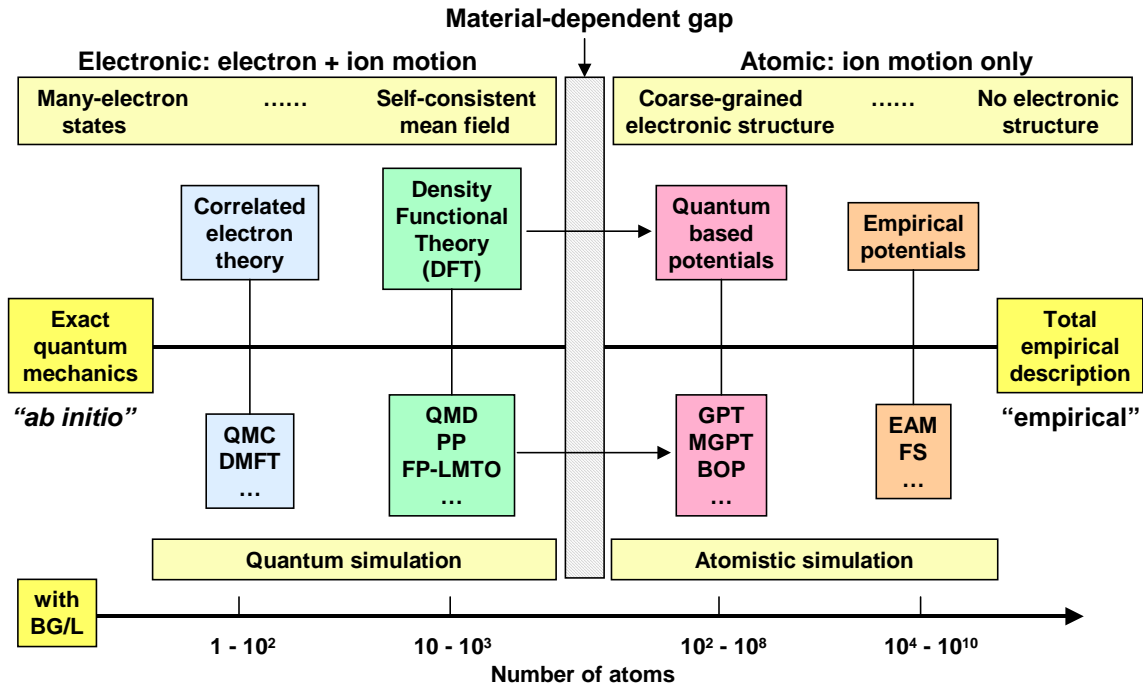


FIG. 1. Representative sample of the wide spectrum of electronic and atomistic simulation approaches used in condensed-matter and materials physics and the material-dependent gap separating them. Indicated are the estimated numbers of transition-metal atoms that could be usefully simulated in each category with LLNL’s new BlueGene/L (BG/L) supercomputer.

quantum-mechanical techniques to classical descriptions with totally empirical force laws. All of these methods fall into one of two distinct categories, which are separated by a *material-dependent gap*. On one side of this gap are electronic methods based on direct quantum-mechanical treatments. These include *quantum simulations* that attempt to treat electron and ion motion on an equal footing, solving quantum-mechanical equations on the fly for both the electronic states of the system and the forces on the individual ions. In transition metals, methods based on density-functional theory (DFT) [2] can provide a highly accurate description of the system and are chemically very robust, but they come at the price of being severely limited in the size and duration of the simulation. On the other side of the gap are methods used in *atomistic simulations*, such as molecular dynamics (MD), that treat only the ion motion, allowing dramatically larger simulations by solving classical Newtonian equations of motion with the forces derived from explicit interatomic potentials. Modeling across the electronic-atomistic gap is possible through the development of first-principles quantum-based potentials based on a systematic *coarse graining* of the DFT electronic structure. We view this as an essential step in the predictive multiscale modeling of real complex materials that we envision here. In this

paper, we present an overview of recent work in the Metals and Alloys Group at Lawrence Livermore National Laboratory (LLNL) on developing robust quantum-based interatomic potentials for transition metals from generalized pseudopotential theory (GPT) and applying these potentials to multiscale modeling simulations.

II. GENERALIZED PSEUDOPOENTIAL THEORY

Within DFT quantum mechanics, first-principles generalized pseudopotential theory provides a fundamental basis for *ab initio* interatomic potentials in both simple and transition metals [3-5]. In the GPT applied to transition metals, a mixed basis of plane waves and localized *d*-state orbitals is used to self-consistently expand the electron density and total energy of the system in terms of weak *sp* pseudopotential, *d-d* tight-binding, and *sp-d* hybridization matrix elements, which in turn are all directly calculable from first principles. For a bulk elemental transition metal, one obtains an explicit real-space total-energy functional of the form [5]

$$E_{tot}(R_1 \dots R_N) = NE_{vol}(\Omega) + \frac{1}{2} \sum'_{i,j} v_2(ij; \Omega) + \frac{1}{6} \sum'_{i,j,k} v_3(ijk; \Omega) + \frac{1}{24} \sum'_{i,j,k,l} v_4(ijkl; \Omega) \quad (1)$$

The leading volume term in this expansion, E_{vol} , as well as the two-, three-, and four-ion interatomic potentials, v_2, v_3 , and v_4 , are volume dependent, *but structure independent* quantities and thus *transferable* to all bulk ion configurations, either ordered or disordered. This includes all structural phases as well as the deformed solid and the imperfect bulk solid with either point or extended defects present. The angular-force multi-ion potentials v_3 and v_4 in Eq. (1) reflect directional-bonding contributions from partially-filled *d* bands and are generally important for mid-period transition metals. In the full *ab initio* GPT, however, these potentials are generally long-ranged, nonanalytic and multidimensional functions, so that v_3 and v_4 cannot be readily tabulated for application purposes. This has led to the development of a simplified and complementary model GPT or MGPT, which achieves for the central transition metals short-ranged, analytic potential forms that can be applied to large-scale atomistic simulations [6,7].

In practice, the *ab initio* GPT and the MGPT have complementary ranges of application. The *ab initio* GPT is most effective in situations where the total-energy expansion (1) can be truncated at the pair-potential level, since tabulation and interpolation of a nonanalytic pair potential $v_2(r, \Omega)$ represents no computational barrier for atomistic simulations. Thus routine *ab initio* GPT applications include *sp*-bonded simple metals, series-end transition metals and appropriate binary alloys, such as the transition-metal aluminides [8]. The primary application range for the MGPT, on the other hand, is the Group-VB and -VIB bcc transition metals such as Ta and Mo. Both GPT and MGPT potentials have been implemented in atomistic simulations and applied to a wide range of bulk structural, thermodynamic, defect and mechanical properties at both ambient and extreme conditions of temperature and pressure [9]. Extension of the

bulk GPT and MGPT potentials to highly nonbulk situations, such as surfaces, voids and clusters, is also possible through appropriate environmental modulation [10].

A. Standard MGPT for central bcc transition metals

The MGPT is derived from the GPT through a series of systematic approximations applicable to mid-period bcc transition metals with nearly half-filled d bands. In the MGPT, long-range interatomic interactions arising from sp - d hybridization are assumed to destructively interfere and are explicitly neglected beyond E_{vol} , while multi-ion d -state non-orthogonality contributions are formally folded back into v_2 . Canonical d bands are introduced to express the remaining d - d tight-binding matrix elements analytically as

$$\langle \phi_d^i | \Delta | \phi_d^j \rangle = \alpha_m f(R_{ij}) = \alpha_m (R_{WS} / R_{ij})^p . \quad (2)$$

For pure canonical d bands $p = 2\ell + 1 = 5$ with $\ell = 2$, but in practice one allows p to be a weakly volume-dependent parameter typically optimized in the range of 4-5, with a Gaussian cutoff introduced beyond the bcc second-neighbor distance [11]. The coefficients α_m are also volume dependent, but in the standard MGPT they are maintained exactly in their canonical d -band ratios of 6 : -4 : 1 for $\alpha_0 : \alpha_1 : \alpha_2$.

The radial-force two-ion pair potential v_2 in the MGPT then consists of simple-metal sp , hard-core overlap and analytic tight-binding d -state contributions:

$$v_2(r, \Omega) = v_2^{sp}(r, \Omega) + v_2^{hc}(r, \Omega) + v_a(\Omega)[f(r)]^4 - v_b(\Omega)[f(r)]^2 . \quad (3)$$

Here the potential contributions v_2^{sp} and v_2^{hc} are retained directly from the *ab initio* GPT, while v_a and v_b are volume-dependent d -state coefficients. The angular-force three- and four-ion potentials v_3 and v_4 are appropriate multi-ion generalizations of the final two terms in Eq. (3). At a given volume Ω , v_3 is a three-dimensional function of the distances linking three ions:

$$v_3(r_1, r_2, r_3; \Omega) = v_c(\Omega) f(r_1) f(r_2) f(r_3) L(\theta_1, \theta_2, \theta_3) + v_d(\Omega) \{ [f(r_1) f(r_2)]^2 P(\theta_3) + [f(r_2) f(r_3)]^2 P(\theta_1) + [f(r_3) f(r_1)]^2 P(\theta_2) \} , \quad (4)$$

while v_4 is a six-dimensional, oscillatory function of the six distances linking four ions:

$$v_4(r_1, r_2, r_3, r_4, r_5, r_6; \Omega) = v_e(\Omega) [f(r_1) f(r_2) f(r_4) f(r_5) M(\theta_1, \theta_2, \theta_3, \theta_4, \theta_5, \theta_6) + f(r_3) f(r_2) f(r_6) f(r_5) M(\theta_7, \theta_8, \theta_9, \theta_{10}, \theta_5, \theta_{12}) + f(r_1) f(r_6) f(r_4) f(r_3) M(\theta_{11}, \theta_{12}, \theta_5, \theta_6, \theta_3, \theta_4)] , \quad (5)$$

where v_c, v_d and v_e are additional volume-dependent d -state coefficients. The quantities L , P and M in Eqs. (4) and (5) are universal angular functions that depend only on d symmetry and apply to all transition metals and all volumes. These functions have exact analytic representations, as given in Ref. [6], and are displayed below in Fig. 7.

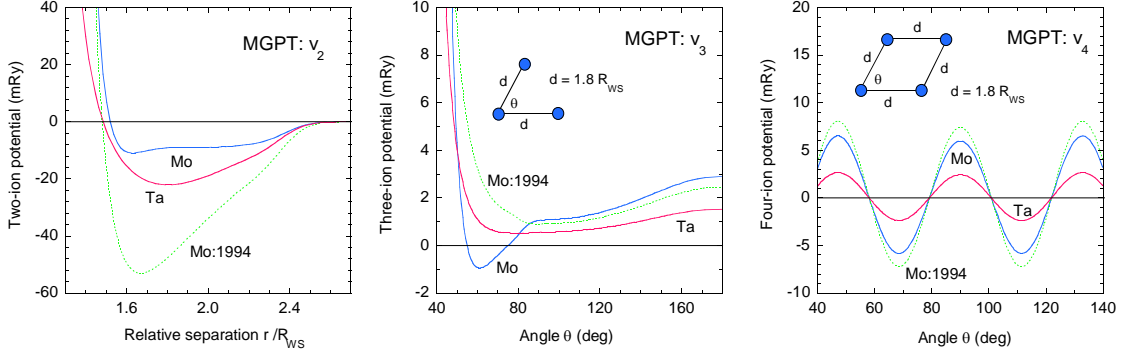


FIG. 2. Optimized MGPT potentials v_2 , v_3 , and v_4 for Ta and Mo at their respective equilibrium volumes. Shown for comparison are earlier 1994 MGPT potentials for Mo.

B. Optimized MGPT potentials for Ta and Mo

The five d -state coefficients v_a, v_b, v_c, v_d and v_e in Eqs. (3)-(5) are all well-defined material parameters that depend primarily on d -band filling and width. To compensate for the approximations introduced into the MGPT, these quantities together with the volume term E_{vol} are parameterized and constrained by basic theoretical and/or experimental data. In our current preferred scheme, we fit as a function of volume a combination of first-principles DFT and experimental data on the cold equation of state, shear elastic moduli, unrelaxed vacancy formation energy and the Debye temperature, under the additional constraint of the compressibility sum rule, which reduces the number of independent parameters from six to five. Optimized Ta MGPT potentials so obtained to 1000 GPa [9,11] are displayed at equilibrium in Fig. 2. Corresponding optimized Mo potentials, recently obtained to 400 GPa [12], are also shown, as are our earlier 1994 Mo potentials [7]. The former potentials are intended to improve upon and replace the latter ones. In this regard, the new MGPT Mo potentials correct known problems with the 1994 potentials at short bond lengths, while giving excellent fcc-bcc and A15-bcc structural energies and improved dislocation properties.

III. SELECTED APPLICATIONS TO MULTISCALE MODELING

The MGPT potentials for Ta and Mo have been applied to a wide range of physical properties at both ambient and extreme conditions, including multiphase equation of state, melting and rapid solidification, high-pressure elastic moduli and ideal strength, thermoelasticity, vacancies and self-interstitials, grain boundaries, and dislocation core structure and mobility. Here we discuss selected recent applications directly relevant to the multiscale modeling of plasticity and strength.

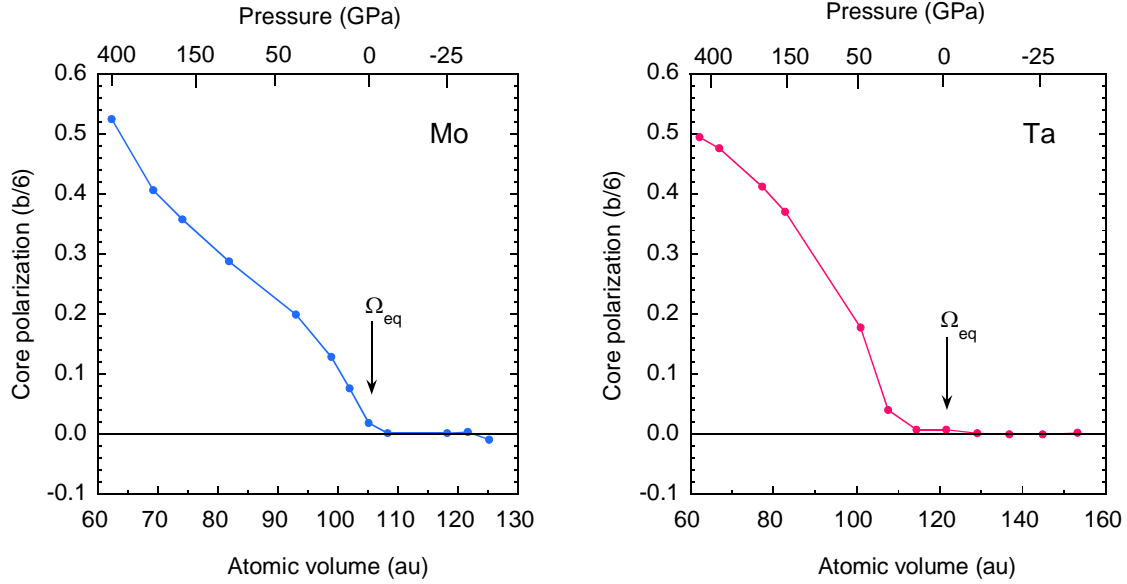


FIG. 3. GF/MGPT core polarization predicted in Mo and Ta as function of volume, giving an isotropic dislocation core near equilibrium and in expansion but a polarized core under pressure.

A. Dislocation core structure and mobility

The low-temperature and high-strain-rate plastic behavior of bcc transition metals is controlled by the intrinsic core properties of $a/2\langle 111 \rangle$ screw dislocations. Unlike the highly mobile edge dislocations in these metals, the motion of the screw dislocations is severely restricted by the non-planar atomic structure of its core, resulting in low mobility, thermal activated kink pairs and a temperature-dependent yield stress.

The accurate atomistic simulation of dislocation core properties has been greatly facilitated by the development of an advanced Green's function (GF) simulation method that allows both static and dynamic calculations [11]. This method implements rigorous flexible boundary conditions by introducing a buffer layer between fixed outer and relaxed inner atomistic regions of the simulation cell, allowing one to dynamically update the boundary conditions as the atoms move. Extensive GF/MGPT simulations have been carried out in Ta and Mo over wide ranges of pressure on the core structure, Peierls stress and its stress-orientation dependence, and kink-pair energetics of $a/2\langle 111 \rangle$ screw dislocations [11,13-15]. In general, the core structure exhibits a three-fold directional spreading, of variable magnitude or polarization \mathbf{p} , along three $\langle 112 \rangle$ directions on three $\{110\}$ planes in the $\langle 111 \rangle$ zone. When \mathbf{p} vanishes, a more symmetric isotropic core is obtained, while at $\mathbf{p} = \pm \mathbf{b}/6$, where \mathbf{b} is the Burgers vector, a fully polarized core with maximum three-fold spreading is obtained. As illustrated in Fig. 3, we predict an isotropic core structure for Mo and Ta near equilibrium and into expansion, but an increasingly polarized core under hydrostatic pressure [15].

Similarly, the Peierls stress τ_p in bcc metals generally exhibits a strong dependence on the orientation of the applied stress and large deviations from the well-known Schmid

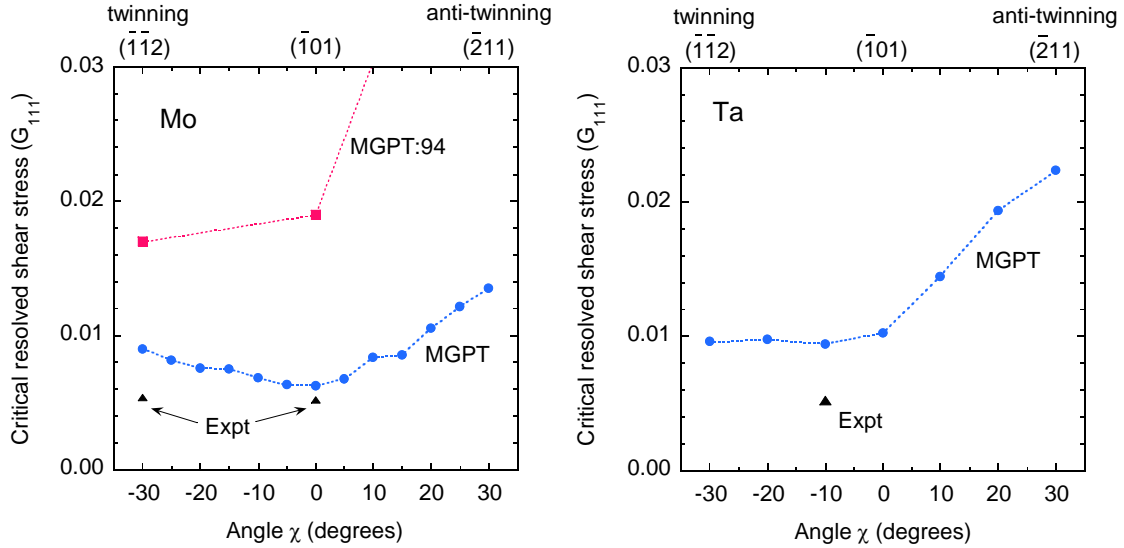


FIG. 4. Peierls stress and its orientation dependence in Mo and Ta at ambient pressure, as calculated with the present MGPT potentials and compared with experimental estimates based on the observed yield stress [16,17] and for Mo with results obtained with the 1994 potentials [18].

law. Figure 4 displays our GF/MGPT predicted Peierls stress in Ta and Mo for a pure applied shear stress as a function of angle χ between twinning and anti-twinning orientations on $\{112\}$ planes [11,15]. The calculated twinning–anti-twinning asymmetry is indicative of non-Schmid behavior, although this is clearly different in the two metals, with τ_p minimum at $\chi = 0^\circ$ for Mo but nearly constant between $\chi = -30^\circ$ and 0° for Ta. Shown for comparison are experimental estimates of the Peierls stress based on extrapolating the observed yield stress to zero temperature [16,17]. Our minimum calculated τ_p in Mo is close to the corresponding estimate, but in the case of Ta is about a factor of two larger. Also in this regard, we believe our present calculated τ_p in Mo is a major improvement over that previously obtained by Rao and Woodward with the 1994 Mo MGPT potentials [18].

B. Atomistically-informed DD simulations of plasticity

At finite temperature, the motion of the $a/2\langle 111 \rangle$ screw dislocations in the bcc lattice normally occurs by the thermally assisted formation and migration of kink pairs. In microscale dislocation dynamics (DD) simulations of single-crystal plasticity for bcc metals [19], a key input quantity is the stress-dependent activation enthalpy for kink-pair formation, $\Delta H(\tau)$. This quantity controls the dislocation mobility, with the stress-dependent velocity of screw dislocation given by

$$v_{screw}(\tau) \propto \exp[-\Delta H(\tau)/k_B T]. \quad (6)$$

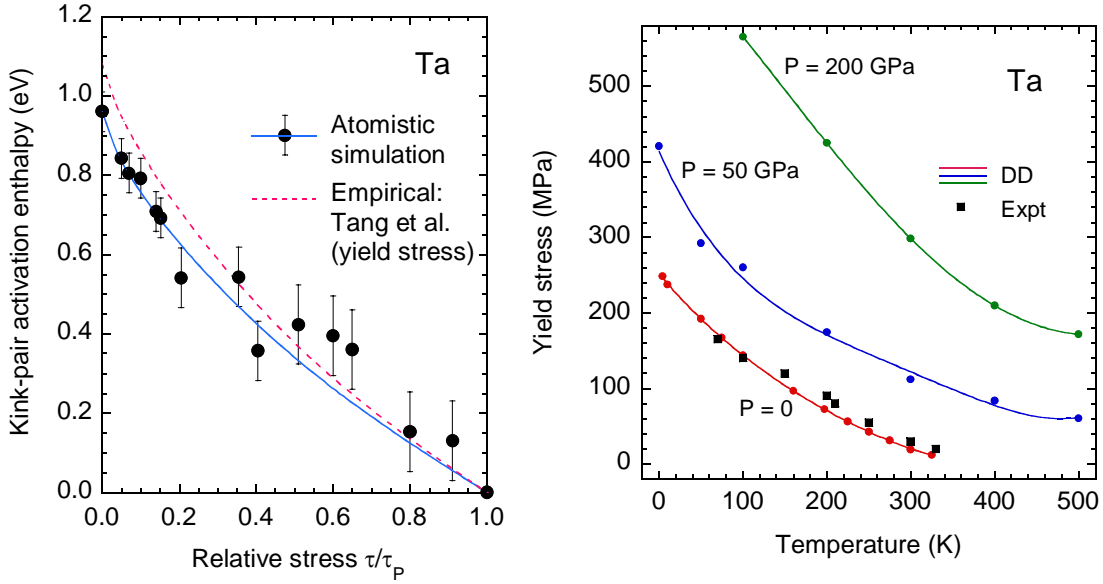


FIG. 5. On the left: simulated GF/MGPT kink-pair activation enthalpy for Ta (points) at ambient pressure, fitted with Eq. (7) (solid line) and compared with the empirical result of Ref. [19] (dashed line). On the right: atomistically-informed DD simulations of the single-crystal yield stress in bcc Ta at three pressures and compared with experiment at ambient pressure [20].

We have now performed extensive GF/MGPT atomistic simulations of $\Delta H(\tau)$ for both Ta and Mo over a wide range of pressures [11,15]. These results can then be fitted to the simple analytic form used in the DD simulations:

$$\Delta H(\tau) = \Delta H(0)[1 - (\tau / \tau_p)^p]^q . \quad (7)$$

One can thereby import the required atomistic information directly into DD simulations for real materials at any assumed pressure condition [14]. In Fig. 5 we display representative atomistic calculations of $\Delta H(\tau)$ in Ta at ambient pressure together with atomistically-informed DD simulations of yield stress as a function of temperature for three selected pressures. In the latter, we have everywhere scaled down the Peierls stress τ_p by about a factor of two to account for the overestimate noted in Fig. 4. Otherwise, the temperature dependence of the yield stress at ambient pressure is in good accord with experiment [20]. Similar DD calculations for Mo have also been performed [15].

C. Thermoelasticity and high-pressure strength modeling

The pressure and temperature dependence of elastic moduli are additional quantities with important implications for strength modeling. In general, we calculate single-crystal moduli C_{ij} as a sum of cold, ion-thermal and electron-thermal components:

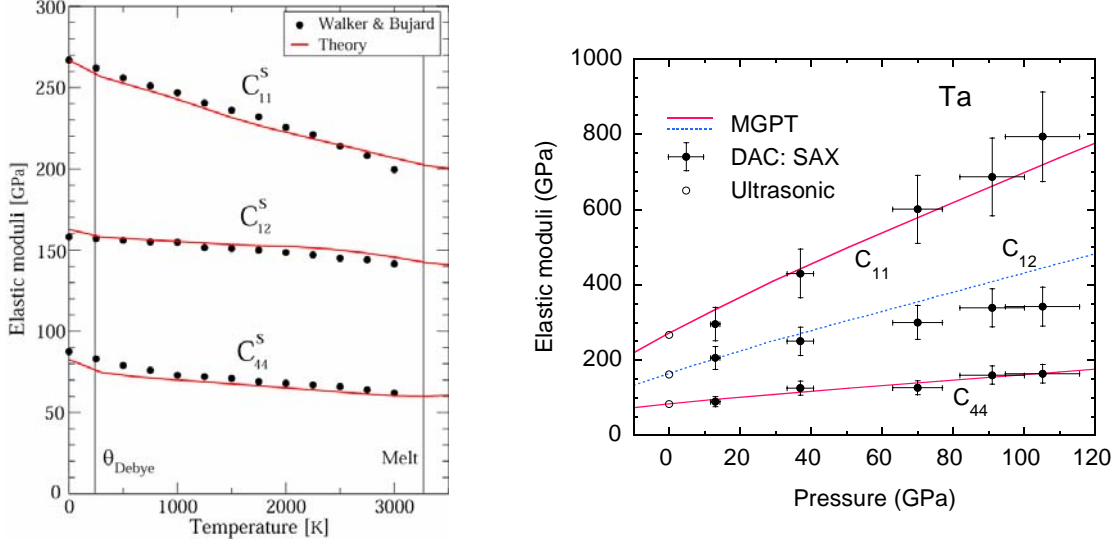


FIG. 6. Present calculated high-temperature and high-pressure elastic moduli (lines) in bcc Ta compared with experiment [23-25] (points): on the left, temperature dependence at ambient pressure; on the right, pressure dependence at ambient temperature.

$$C_{ij}(P, T) = C_{ij}^0(P) + C_{ij}^{ion}(P, T) + C_{ij}^{el}(P, T) . \quad (8)$$

The cold component C_{ij}^0 is taken from DFT calculations or experiment and the electron-thermal component C_{ij}^{el} from DFT calculations at finite temperature, while the remaining ion-thermal component C_{ij}^{ion} is obtained from strain derivatives of phonons calculated using MGPT potentials. We have, in fact, developed two useful MGPT-based methods to obtain C_{ij}^{ion} [21]. The first involves a standard quasi-harmonic-phonon formalism with the calculation of explicit strain derivatives, while the second involves more time consuming Monte Carlo simulation and the statistical evaluation of appropriate fluctuation formulae. The latter includes both quasi-harmonic and anharmonic contributions to C_{ij}^{ion} . We have used these methods to investigate the full thermoelastic behavior of Ta and Mo at high-temperature and pressure [21], building on previous studies of the cold high-pressure elastic moduli in Ta [9,22]. A sample of these results for Ta is displayed in Fig. 6 and compared with available experimental data [23-25]. In this case, anharmonic effects are found to be small and the observed temperature dependence of the elastic moduli at ambient-pressure [23] is well described by both our quasi-harmonic and Monte Carlo methods. Accurate experimental moduli are also known at very low pressure from ultrasonic measurements [24] and have recently been measured in the diamond-anvil cell (DAC) to 105 GPa with a stress/angle-resolved x-ray diffraction (SAX) technique [25].

Many continuum-level materials strength models, such as the well know Steinberg-Guinan (SG) model [26], use the macroscopic shear modulus $G(P, T)$ to scale strength data from near ambient conditions to high pressures and temperatures. With appropriate polycrystalline averaging, our single-crystal moduli can be used to calculate $G(P, T)$ and

in turn, to either validate or improve upon existing empirical models of the shear modulus. In the case of Ta, the SG model of $G(P,300K)$ has thereby been validated to 1000 GPa. More generally, we have investigated the validity of the assumed linear scaling of strength with shear modulus. In Ta and Mo we find that both the ideal shear strength of the bcc perfect crystal and the Peierls stress τ_p for $a/2\langle 111 \rangle$ screw dislocations display approximate linear scaling with $G_{111} = (2C' + C_{44})/3$, the shear modulus in the $\langle 111 \rangle$ direction, to 1000 and 400 GPa, respectively [15].

IV. BEYOND THE STANDARD APPROACH: MATRIX MGPT

One of the great virtues of the underlying first-principles GPT formalism for interatomic potentials is that it allows one to systematically improve the model GPT in a manner consistent with quantum mechanics. Recently, we have made major strides in this direction by developing a more general matrix MGPT representation. In the matrix MGPT, the three- and four-ion angular functions P , L and M in Eqs. (4) and (5) are recast as matrix products that can be evaluated on the fly numerically during a simulation:

$$P \propto \text{Tr}(\hat{H}_{ij}\hat{H}_{ji}\hat{H}_{ik}\hat{H}_{ki}), \quad L \propto \text{Tr}(\hat{H}_{ij}\hat{H}_{jk}\hat{H}_{ki}) \quad \text{and} \quad M \propto \text{Tr}(\hat{H}_{ij}\hat{H}_{jk}\hat{H}_{kl}\hat{H}_{li}). \quad (9)$$

For transition metals \hat{H}_{ij} is a normalized and explicit 5×5 d -state matrix coupling sites i and j . In this representation, several major extensions of the standard MGPT are possible. First, the matrix elements of \hat{H}_{ij} can be immediately generalized to treat non-canonical d -bands with arbitrary tight-binding coefficients α_m in Eq. (2), resulting in two additional MGPT parameters α_0/α_2 and α_1/α_2 , but otherwise with no added complication to the theory. Second, one may further generalize from d states to f states to treat actinide metals, in which case \hat{H}_{ij} becomes a 7×7 matrix. The form of the f -state matrix may be readily derived from the general two-center Slater-Koster tight-binding integrals [27]. For canonical f -bands, one has $p = 2\ell + 1 = 7$ with $\ell = 3$ and ratios of $20 : -15 : 6 : -1$ for $\alpha_0 : \alpha_1 : \alpha_2 : \alpha_3$. The corresponding angular functions P , L and M for

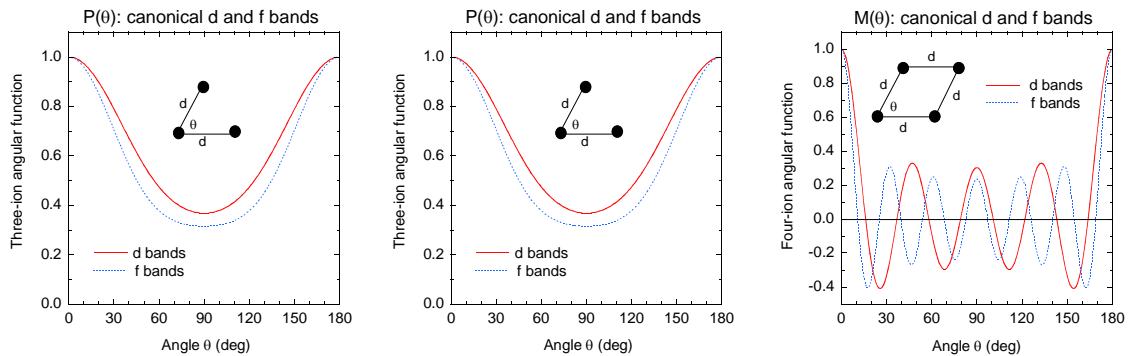


FIG. 7. MGPT three- and four-ion angular functions P , L and M for canonical d and f bands.

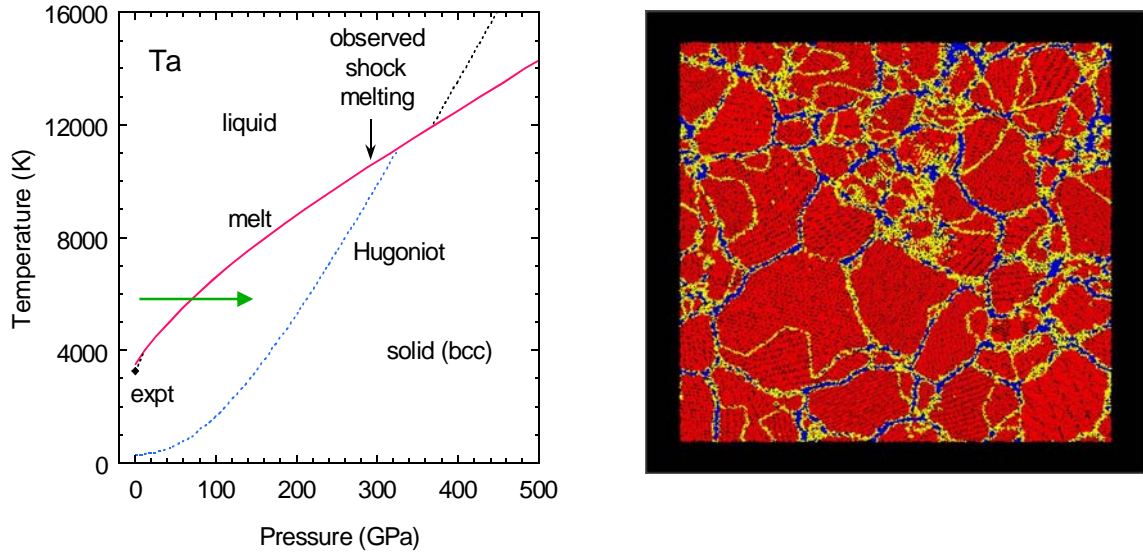


FIG. 8. Rapid solidification in Ta. On the left: isothermal compression path (arrow) across the high-pressure MGPT melt curve. On the right: snapshot of a 16-million atom MD/MGPT solidification simulation after 0.5 ns showing a rich emerging grain microstructure [29].

canonical f bands are displayed in Fig. 7 and compared with those for canonical d bands. The function P for three-ion interactions is little changed, but quantum mechanics has added an extra oscillation in both L and M for f bands.

A third major advance that has been facilitated by the matrix MGPT concerns computational efficiency. The matrix representation has proved to be amenable to a number of algorithm improvements in the evaluation of energies and forces, most notably an optimized strategy to calculate the multi-ion energy terms in Eq. (1) and an explicit analytic treatment of the forces [28]. This has resulted in MGPT simulation codes that are 6-10 times faster and has dramatically increased the size and scope of problems that can be addressed on large parallel platforms. The most striking example of this is the very recent large-scale MD/MGPT simulations of rapid solidification in Ta that have been performed on LLNL's new BlueGene/L (BG/L) supercomputer [29]. In this problem, one is rapidly compressing a hot molten metal across the high-pressure melt curve, and one seeks to understand the time scale and kinetics of the solidification transition as well as the atomic and microscale morphology of the resolidified solid. Prior to BG/L, the size of the simulations ($\sim 10,000$ atoms) that could be run for the required time (~ 1 ns) was two orders of magnitude smaller than needed to access the required physics. With BG/L, this threshold has been passed with ease and successful Ta simulations up to 32 million atoms have been performed that predict a rich and complex early-time grain microstructure, as illustrated in Fig. 8.

Using the f -electron matrix representation of MGPT, we have made additional applications to the actinide metals U and δ -phase (fcc) Pu. Preliminary potentials based on canonical bands for these metals are displayed in Fig. 9 at equilibrium. In the case of

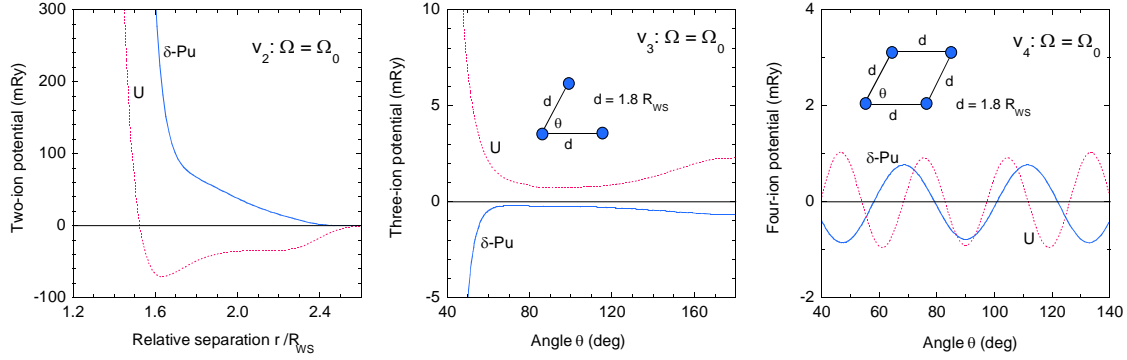


FIG. 9. Preliminary MGPT potentials $v_2, v_3,$ and v_4 for the actinide metals U and δ -Pu at their respective equilibrium volumes, calculated with canonical f and d bands, respectively.

U, the potentials have been calculated to 100 GPa and applied to study structural phase stability in that pressure range. If one allows the value of the p parameter in the radial function $f(r)$ to be reduced from its canonical value of 7 to the vicinity of 4, a good account is obtained for structural energy differences between the observed α -U orthorhombic phase and other common structures. Unfortunately, we have discovered that the α -U structure itself is not mechanically stable in this treatment and that there are other lower-energy orthorhombic structures. This possibly signals missing physics, such as neglected spd - f hybridization and/or higher-order five- and six-ion interactions, since U has only about a quarter f -band filling instead of the half f -band filling implicitly assumed in the MGPT.

The case of δ -Pu is not ideal either because of strong f -electron correlation, but for this metal we have managed to develop a useful practical scheme. Here we have modeled the strong correlation very simply by assuming that it turns off the f -electron bonding completely, so that δ -Pu can be described as a d -band metal in the context of MGPT. This seems to be rather successful, and both the structural phase stability and the full fcc phonon spectrum are reasonably well described by this treatment, as shown in Fig. 10. In particular, in a d -bonding MGPT treatment the observed fcc structure is both mechanically stable and of lowest energy, whereas in an f -bonding treatment, a bct structure has a substantially lower energy. The calculated phonons from the d -bonding treatment also compare well with recent experimental measurements [30], except for the anomalous low-frequency transverse branch in the $\langle 111 \rangle$ direction ($\Gamma \rightarrow L$ in Fig. 10).

Two other important areas we are currently pursuing are the use of non-canonical bands and the development of temperature-dependent MGPT potentials. In principle, non-canonical bands permit a more accurate characterization of the underlying electronic structure. In practice, we have found them useful in improving the overall quality of the calculated phonon spectrum in certain difficult cases such as Mo. Interestingly, the introduction of just two non-canonical band parameters seems to be able to improve *all* phonons at *all* volumes.

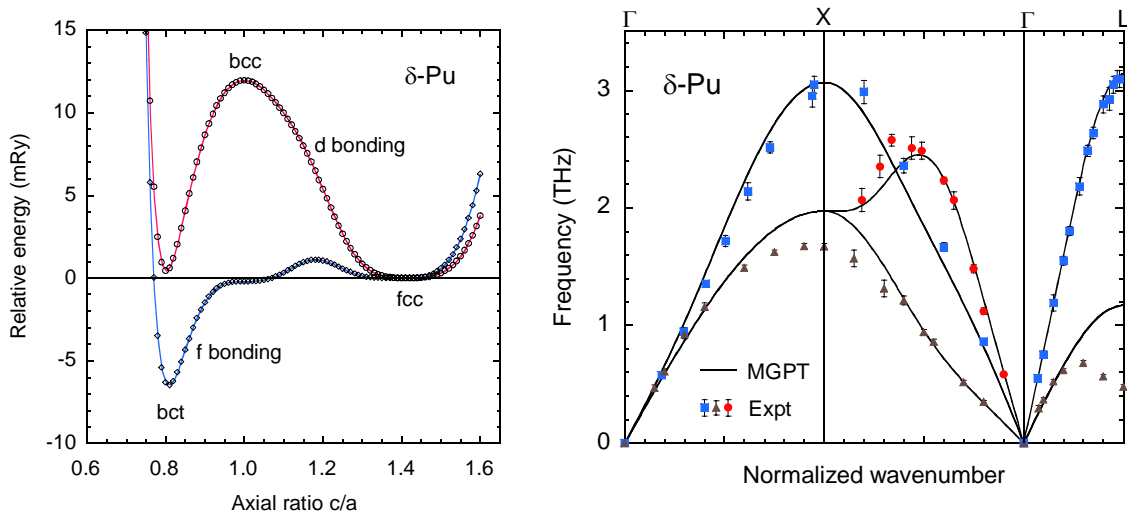


FIG. 10. Phase stability and phonons in δ -Pu. On the left: structural energies along the Bain path at constant volume in both d - and f -bonding MGPT treatments. On the right: MGPT phonons calculated from the d -bonding treatment compared against experiment [30].

The concept of temperature-dependent potentials for d - and f -electron metals is an important one, because in such metals there are large electron-thermal effects at temperatures as low as melt arising from the high density of electronic states at the Fermi level. These effects can have a dramatic impact on high-temperature properties including the melt curve itself [7], but are normally treated separately and additively from the normal ion-thermal effects, as in Eq. (8). We are now trying to capture these effects simultaneously and self-consistently by building MGPT potentials on the basis of the total electron free energy at finite temperature.

One final additional future application area made possible by the matrix MGPT should also be mentioned. That is the possibility of extending the total-energy expansion in Eq. (1) beyond four-ion interactions. We believe that it is now feasible to include both five- and six-ion potentials in the MGPT. This should improve the description of certain structural properties, such as close-packed energy differences and stacking faults, and permit a more accurate treatment of metals to either side of the mid-period transitions elements. It may also improve the description of the observed complex structures in the early actinide metals as well.

ACKNOWLEDGMENT

This work was performed under the auspices of the U.S. Department of Energy by the University of California Lawrence Livermore National Laboratory under contract number W-7405-ENG-48.

REFERENCES

1. See, for example, J. A. Moriarty, V. Vitek, V. V. Bulatov and S. Yip: Atomistic simulations of dislocations and defects. *J. of Computer-Aided Mater. Design* **9**, 99 (2002) and references therein.
2. P. Hohenberg and W. Kohn: Inhomogeneous electron gas. *Phys. Rev.* **136**, B864 (1964); W. Kohn and L. J. Sham: Self-consistent equations including exchange and correlation effects. *Phys. Rev.* **140**, A1133 (1965).
3. J. A. Moriarty: Density-functional formulation of the generalized pseudopotential theory. *Phys. Rev. B* **16**, 2537 (1977).
4. J. A. Moriarty: Density-functional formulation of the generalized pseudopotential theory. II. *Phys. Rev. B* **26**, 1754 (1982).
5. J. A. Moriarty: Density-functional formulation of the generalized pseudopotential theory. III. Transition-metal interatomic potentials. *Phys. Rev. B* **38**, 3199 (1988).
6. J. A. Moriarty: Analytic representation of multi-ion interatomic potentials in transition metals. *Phys. Rev. B* **42**, 1609 (1990).
7. J. A. Moriarty: Angular forces and melting in bcc transition metals: A case study of molybdenum. *Phys. Rev. B* **49**, 12431 (1994).
8. J. A. Moriarty and M. Widom: First-principles interatomic potentials for transition-metal aluminides: Theory and trends across the 3d series. *Phys. Rev. B* **56**, 7905 (1997).
9. J. A. Moriarty, J. F. Belak, R. E. Rudd, P. Söderlind, F. H. Streitz and L. H. Yang: Quantum-based atomistic simulation of materials properties in transition metals. *J. Phys.: Condens. Matter* **14**, 2825 (2002).
10. J. A. Moriarty and R. Phillips: First-principles interatomic potentials for transition-metal surfaces. *Phys. Rev. Lett.* **66**, 3036 (1991).
11. L. H. Yang, P. Söderlind and J. A. Moriarty: Accurate atomistic simulation of $a/2\langle 111 \rangle$ screw dislocations and other defects in bcc tantalum. *Philos. Mag. A* **81**, 1355 (2001).
12. J. A. Moriarty, unpublished.
13. L. H. Yang, P. Söderlind and J. A. Moriarty: Atomistic simulation of pressure-dependent screw dislocation properties in bcc tantalum. *Mater. Sci. Eng. A* **309-310**, 102 (2001).
14. L. H. Yang and J. A. Moriarty: Kink-pair mechanisms for $a/2\langle 111 \rangle$ screw dislocation motion in bcc tantalum. *Mater. Sci. Eng. A* **319-321**, 124 (2001).
15. L. H. Yang, P. Söderlind, M. Tang and J. A. Moriarty (to be published).
16. A. Seeger and L. Hollang: The flow-stress asymmetry of ultra-pure molybdenum single crystals. *Materials Transactions JIM* **41**, 141 (2000) and L. Hollang, M. Hommel and A. Seeger: The flow stress of ultra-high-purity molybdenum single crystals. *Phys. Stat. Sol. (a)* **160**, 329 (1997).
17. T. Suzuki, Y. Kaminura and H. O. K. Kirchner: Plastic homology of bcc metals. *Philos. Mag. A* **79**, 1629 (1999).

18. S. Rao and C. Woodward: Atomistic simulations of $(a/2)\langle 111 \rangle$ screw dislocations in bcc Mo using a model generalized pseudopotential theory potential. *Philos. Mag. A* **81**, 1317 (2001).
19. M. Tang, L. P. Kubin and G. R. Canova: Dislocation mobility and the mechanical response of bcc single crystals: A mesoscopic approach. *Acta mater.* **46**, 3221 (1998).
20. W. Wasserbäch: Plastic deformation and dislocation arrangement of Nb-34at% Ta alloy single crystals. *Philos. Mag. A* **53**, 335 (1986).
21. D. A. Orlikowski, P. Söderlind and J. A. Moriarty (to be published).
22. P. Söderlind and J. A. Moriarty: First-principles theory of Ta up to 10 Mbar pressure: Structural and mechanical properties. *Phys. Rev. B* **57**, 10340 (1998).
23. E. Walker and P. Bujard: Anomalous temperature behavior of the shear elastic constant C_{44} in tantalum. *Solid State Commun.* **34**, 691 (1980).
24. K. W. Katahara, M. H. Manghnani and E. S. Fisher: Pressure derivatives of the elastic moduli of bcc Ti-V-Cr, Nb-Mo and Ta-W alloys. *J. Phys. F: Metal Phys.* **9**, 773 (1979).
25. H. Cynn and C.-S. Yoo: Single crystal elastic constants of tantalum to 105 GPa. Lawrence Livermore National Laboratory report UCRL-JC-137930 (2000).
26. D. J. Steinberg, S. G. Cochran and J. Guinan: A constitutive model for metals applicable at high-strain rate. *J. Appl. Phys.* **51**, 1498 (1980).
27. A. K. McMahan: Two-center s - f Slater-Koster integrals. *Phys. Rev. B* **58**, 4293 (1998).
28. J. N. Glosli, unpublished.
29. F. H. Streitz, J. N. Glosli and M. V. Patel: Beyond finite-size scaling: Modeling of molten Ta on BlueGene/L (to be published).
30. J. Wong, M. Krisch, D. L. Farber, F. Occelli, A. J. Schwartz, T.-C. Chiang, M. Wall, C. Boro and R. Xu: Phonon dispersions of fcc δ -plutonium-gallium by inelastic x-ray scattering. *Science* **301**, 1078 (2003).